Available online at www.sciencedirect.com
ScienceDirect
Journal of Power Sources 163 (2007) 882–891
JOURNAL OF POWER SOURCES
www.elsevier.com/locate/jpowsour

Flow rate and humidification effects on a PEM fuel cell performance and operation

Galip H. Guvelioglu *, Harvey G. Stenger

Chemical Engineering Department, Lehigh University, Bethlehem, PA 18015, USA

Received 4 August 2006; received in revised form 19 September 2006; accepted 20 September 2006
Available online 13 November 2006

Abstract

A new algorithm is presented to integrate component balances along polymer electrolyte membrane fuel cell (PEMFC) channels to obtain three-dimensional results from a detailed two-dimensional finite element model. The analysis studies the cell performance at various hydrogen flow rates, air flow rates and humidification levels. This analysis shows that hydrogen and air flow rates and their relative humidity are critical to current density, membrane dry-out, and electrode flooding. Uniform current densities along the channels are known to be critical for thermal management and fuel cell life. This approach, of integrating a detailed two-dimensional across-the-channel model, is a promising method for fuel cell design due to its low computational cost compared to three-dimensional computational fluid dynamics models, its applicability to a wide range of fuel cell designs, and its ease of extending to fuel cell stack models.

Keywords: PEM fuel cell; Flow rate; Humidification; Relative humidity; Fuel cell performance

1. Introduction

Fuel cell design and technology are critical research areas necessary for the transition to a hydrogen economy. There are several different fuel cell technologies, polymer electrolyte membrane fuel cell (PEMFC), alkaline fuel cell (AFC), phosphoric acid fuel cell (PAFC), molten carbonate fuel cell (MCFC) and solid oxide fuel cell (SOFC) each with different designs, chemistries and operating conditions [1]. PEMFC's stand out from other fuel cell technologies due to their higher current densities, use of a solid polymer membrane for the cell electrolyte, and low temperature operation (60–90 °C). By using a solid polymer electrolyte the problems associated with sealing, handling, and assembly of corrosive electrolytes used in the other fuel cell technologies are avoided. Furthermore the low temperature operation of PEMFC makes them suitable for use in mobile, transportation and backup power systems due to their fast start-up times, easier thermal management and overall system weight [1,2]. The major challenges facing commercialization of the PEMFC are the cost, reliability and life [1,3].

Mathematical models and simulations are used extensively by researchers to overcome the engineering challenges of commercializing PEMFC's. A significant amount of research has been aimed at increasing the understanding of PEMFC physics through modeling. It is beyond the scope of this paper to review all of the models; a detailed review of the available fuel cell models and their comparisons is available elsewhere (Haraldsson and Wipke [4]).

The models developed by researchers have evolved from one-dimensional "along-the-channel" forms [5–7] to more realistic two-dimensional models of the flow channels and a fundamental representation of the membrane electrode assembly (MEA) (Gurau et al. [8]). With the aid of computational fluid dynamics (CFD) software packages in late 1990s, the fuel cell modelers began developing three-dimensional CFD models [9–13]. The earlier two-dimensional models were mostly along-the-channel models and the effects of bipolar plate shoulders and channel sizes were not studied. The three-dimensional CFD models solved this limitation by adding the across the channel third dimension.

Commercial fuel cell anode and cathode catalyst layer thicknesses are on the order of 10–20 μm and the height and width of the single cell in a stack are 10–20 cm. These dimension mismatches require at least a million elements to model even

* Corresponding author. Tel.: +1 610 481 5926; fax: +1 610 481 6288.
E-mail address: galip@lehigh.edu (G.H. Guvelioglu).

0378-7753/$ – see front matter © 2006 Elsevier B.V. All rights reserved.
doi:10.1016/j.jpowsour.2006.09.052

Nomenclature

c_w	mass concentration of water in the membrane (kg m^{-3})
D_w	water diffusivity (m^2 s^{-1})
F_i	flow rate
F	Faraday's constant, 96487 C (mol^{-1})
n_d	drag coefficient
N_w	water flux (mol m^{-2} s^{-1})
p	pressure (Pa)
t	thickness (m)
V_{cell}	cell operating potential (V)
W	width (m)
x	mole fraction

Greek letters

σ	conductivity (S m^{-1})
ϕ	potential (V)
ε	porosity

Subscripts

a	anode
c	cathode
GDE	gas distribution electrode
i	components, H_2, and H_2O for the anode, O_2, H_2O, and N_2 for the cathode
l	liquid water
m	membrane
w	water in the membrane

Superscripts

0	boundary condition

a small 7 cm × 1 cm section of a fuel cell, and can take more than 1 h with a 10–50 node parallel computer [13]. Although the recent modeling trend is three-dimensional CFD PEMFC models, in our previous work [14], we developed a two-dimensional across-the-channel CFD PEM fuel cell model where the effects of channel and bipolar plate dimensions as well as the properties of the fuel cell components were studied for various given conditions. By using a two-dimensional across-the-channel model we were able to study the effects of cell design and operating conditions rapidly and accurately.

In later work [15], we used the two-dimensional finite element model and a design-of-experiments approach to study the main and interaction effects of five key design factors. These factors included: channel size, shoulder size, gas distribution electrode (GDE) thickness, GDE porosity, and GDE conductivity. These were all studied at moderate and high current density operations. An interaction is defined as the failure of a factor to produce the same response at different levels of another factor. Strong interactions between design factors that effect mass transport were identified and quantified which will aid researchers in the design of PEMFCs. Because the approach used was an across-the-channel model, it did not study the concentration change effects along the channel. To observe those effects the analysis was run for the inlet and exit fuel cell gas concentrations. The results of that work showed that the interactions between design factors become more significant at the exit conditions of the fuel cell.

For a given design, fuel cell performance depends strongly on operating conditions. The effects of operating temperature and pressure have been studied by various researchers with mathematical models [9,16]. The range of these operating parameters is limited by the physical and chemical limitations of the PEMFC materials.

To achieve the maximum power thus reducing the cost per kW, a major challenge is water management. The fuel cell must be operated such that the membrane is adequately hydrated to reduce the ohmic losses. Also the water generated at the cathode must be removed quickly too avoid electrode flooding. Recent work by others has focused on humidification levels and flow rates of hydrogen and air. Berning and Djilali [17] developed a two-phase (liquid–gas) model, of the porous GDE and the gas channel of a PEMFC but excluded the MEA. Water transport through the MEA was therefore ignored. Recently, Pasaogullari and Wang [18] conducted a comprehensive study on the stoichiometry and humidification requirements of PEMFC operation using a two-phase model. Their work showed that flow rates and humidification are key parameters for highly efficient fuel cells. The ratio of reactant available divided by the amount of reactant required for the desired current density (stoichiometric ratio), is also a critical operating condition as it determines the efficiency of the fuel cell. Feed flow rates of hydrogen and water are also critical parameters to manage water in the fuel cell itself and fuel cell system [19]. Berning and Djilali [17] also studied the effects of stoichiometric ratio on performance but because their model assumes constant membrane water content, it could not answer the water management questions.

Even though our two-dimensional across-the-channel finite element model [14] is fast and detailed, it lacks the ability to study the effects of concentration changes along the channel. This is a significant limitation when studying the flow rate and humidification requirements. In this study, a simple Euler integration method has been added to the two-dimensional model to solve the problem of flow of reactants along the channel. With the algorithm developed in this study the performance of the fuel cell can be evaluated in a fraction of the time of a comparable three-dimensional model. This increased speed allows the model to be used as a design tool, not just an analysis tool.

2. Two-dimensional model

The across-the-channel model used in this study was published earlier [14]. It assumes:

- Steady-state operation,
- isothermal operation,
- ideal gas mixtures,
- single phase model,
- isotropic and homogeneous electrodes and membrane,
- the membrane is considered impermeable for the gas phase,

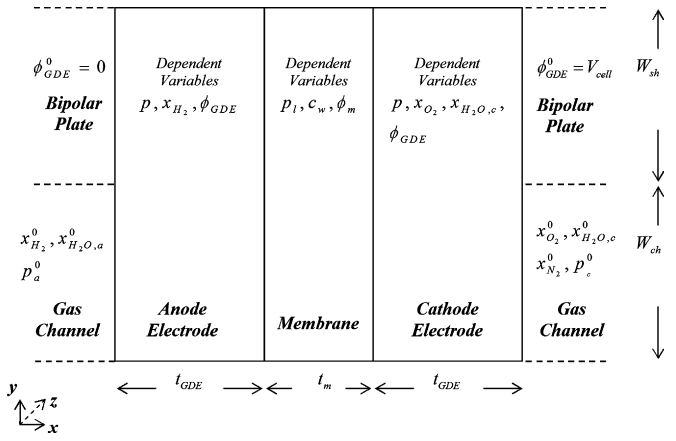

Fig. 1. The dependent variables, boundary conditions, and computational domain.

- negligible contact resistance,
- minimal membrane swelling.

The anode and cathode catalyst layers are modeled as reactive boundaries because their thickness of 10–25 μm is significantly smaller than all other component thicknesses. The remainder of the fuel cell model is a comprehensive two-dimensional, isothermal, steady-state model providing a detailed description of the following transport phenomena:

- Multi-component flow,
- diffusion of reactants through the porous electrodes,
- electrochemical reactions,
- transport of electrons through the electrodes,
- water balance in the membrane.

The equations governing these processes include:

- Ionic balance in electrodes and membrane, ϕ_{GDE} and ϕ_m,
- the Maxwell–Stefan equations for multi-component diffusion and convection in gas distribution channels and gas distribution layers, x_{H_2}, x_{O_2}, and $x_{H_2O,c}$,
- Darcy's law for the flow of species in porous electrodes, p,
- water balance and water flux in the membrane governed by diffusion, convection and electro-osmotic drag, p_l and c_w.

The domain, dependent variables and boundary conditions are outlined in Fig. 1, details of the model can be found in Guvelioglu and Stenger [14].

FEMLAB® a finite element computational fluid dynamics package, was used to solve the nonlinear system of equations. The model was first created and tested in FEMLAB®'s graphical user interface and then saved as a MATLAB® m-file [20]. Details of the model, geometry meshing and solver settings were presented previously [14].

3. Two-dimension to three-dimension integration

The anode and cathode channels have three face boundaries where components can enter or leave, these are channel entrance, channel exit, and channel-GDE boundary. Control volumes for both anode and cathodes are chosen that include the channels and GDE's at each side of the channel.

The algorithm for solving the problem is shown in Fig. 2. To simulate a three-dimensional model first the inlet flow rate of components are calculated. Because the velocity profiles in the channels are not modeled, the pressure drop along-the-channel is neglected. Due to the high flow rates and small channels widths and heights, concentration gradients across the gas channel (x- and y-directions) are neglected. The transport of the components

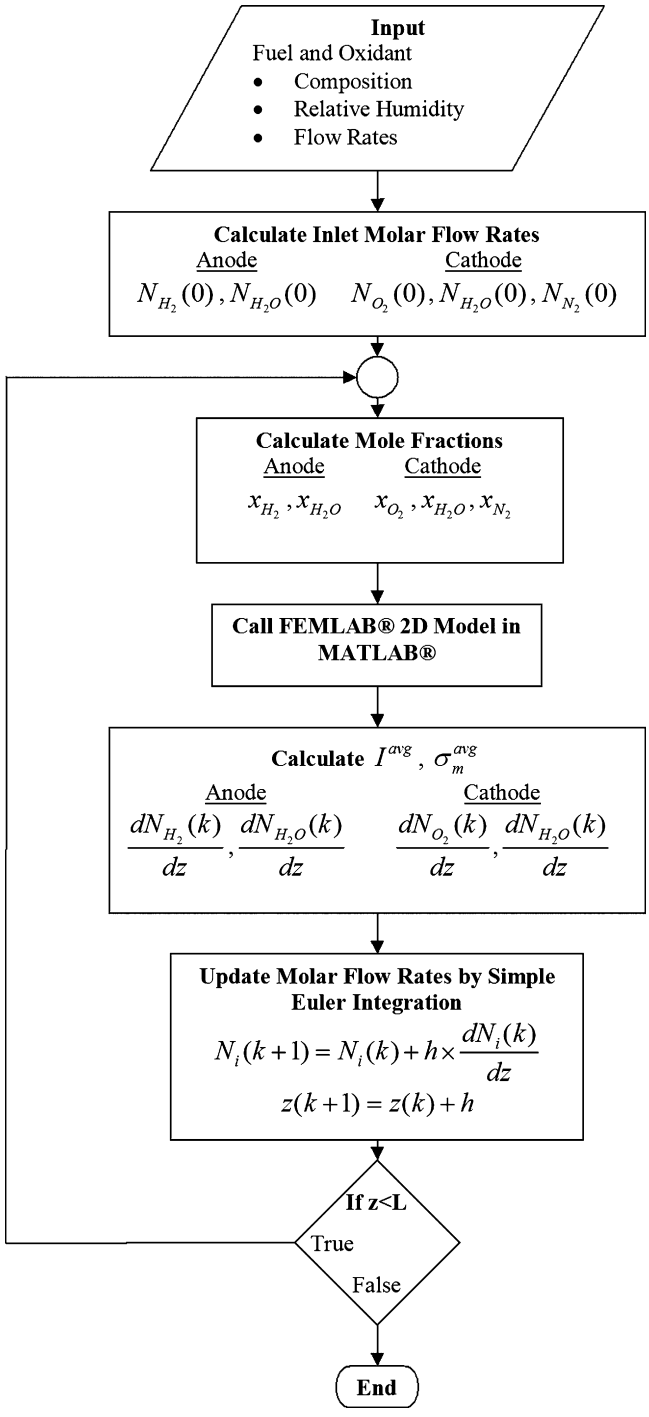

Fig. 2. Two-dimension to three-dimension integration algorithm.

in the GDE's as well as water in the membrane along the channel (z-direction) is neglected due to the order of magnitude difference in dimensions of the channel width and height versus the length.

The inlet mass flow rates are calculated based on the specified flow rate, where F_a is the anode flow rate and is equal to 1.0 when the hydrogen flow rate is sufficient to produce 1 A cm^{-2}.

For the anode, the inlet flow rate of hydrogen is calculated with the following equation:

$$N_{H_2}(0) = F_a \times \frac{1 \times 10^4 \times (W_{sh} + W_{ch}) \times L}{2 \times F} \quad (1)$$

where W_{sh} and W_{ch} are the shoulder and channel widths, L the length of the channel and F is Faraday's constant.

For inlet compositions, the water mole fraction is calculated from the relative humidity (RH):

$$x_{H_2O,a} = \frac{p_{sat} \times RH_a}{p_a} \quad (2)$$

where RH_a is the relative humidity of the anode stream, p_a the anode operating pressure, p_{sat} is the saturation pressure of water calculated with [21]:

$$p_{sat} = \exp\left(73.648 - \frac{7258.2}{T} - 7.3037 \log T + 4.1653 \times 10^{-6} T^2\right) \quad (3)$$

After the water mole fraction at the anode is calculated the molar flow rate of water is calculated by Eq. (4):

$$N_{H_2O,a}(0) = \frac{x_{H_2O} \times N_{H_2}}{(1 - x_{H_2O})} \quad (4)$$

The cathode flow rates are calculated similar to the anode. The flow rate, F_c is used and is equal to 1.0 when the oxygen flow rate is sufficient to generate 1 A cm^{-2}.

$$N_{O_2}(0) = F_c \times \frac{1 \times 10^4 \times (W_{sh} + W_{ch}) \times L}{4 \times F} \quad (5)$$

The inlet nitrogen molar flow rate is calculated using oxygen molar flow rate and the composition of air before humidification.

$$N_{N_2}(0) = \frac{N_{O_2} \times 0.79}{0.21} \quad (6)$$

The water mole fraction is calculated by:

$$x_{H_2O,c} = \frac{p_{sat} \times RH_c}{p_c} \quad (7)$$

And the inlet water molar flow rate for the cathode side is calculated by:

$$N_{H_2O,c}(0) = \frac{x_{H_2O,c} \times (N_{O_2} + N_{N_2})}{(1 - x_{H_2O})} \quad (8)$$

Once the flow rates of the components are calculated the mole fractions of components are used as boundary conditions for the GDE-gas channel interface for the two-dimensional model as shown in Fig. 1. The two-dimensional model is then used to solve mass, momentum and charge balances. The eight dependent variables, p, p_l, c_w, x_{H_2}, x_{O_2}, $x_{H_2O,c}$, ϕ_{GDE} and ϕ_m are then obtained in the computational domain.

A control volume is selected that includes both the gas channel and the GDE. The total flux of hydrogen and water at the anode catalyst-GDE boundary and the total flux of oxygen and water at the cathode catalyst-GDE boundary ($W_{sh} + W_{ch}$) as shown in Fig. 1, is calculated by integrating the flux values along the boundary.

$$\frac{dN_i(k)}{dz} = \int_0^{W_{sh}+W_{ch}} j_i(y)\, dy \quad (9)$$

where j_i is the molar flux of component i, and i is equal to H_2 and H_2O for the anode and O_2 and H_2O for the cathode. The gradient of the flux of N_2 is zero because the membrane is impermeable to all components except water. The average current density is calculated by integrating the local current density along the catalyst layer as shown in Eq. (10).

$$I^{avg} = \frac{1}{W_{sh} + W_{ch}} \int_0^{W_{sh}+W_{ch}} I(y)\, dy \quad (10)$$

For further insight, the average conductivity of the membrane is calculated by integrating the membrane conductivity and dividing it by the membrane area.

$$\sigma_m^{avg} = \frac{1}{(W_{sh} + W_{ch}) \cdot t_m} \int_0^{W_{sh}+W_{ch}} \int_0^{t_m} \sigma_m(x, y) \cdot dx \cdot dy \quad (11)$$

Table 1
Base case geometric parameters

Parameter	Value
W_{ch}, the gas channel width (m)	7.62×10^{-4}
W_{sh}, the bipolar shoulder width (m)	7.62×10^{-4}
L, channel length (m)	0.1
t_{GDE}, anode and cathode GDE thickness (m)	3×10^{-4}
t_m, membrane thickness (m)	1.78×10^{-4}
ε_{GDE}, GDE porosity of the anode and cathode	0.6

Table 2
Operating condition parameters

Symbol	Value
V_{cell}, cell potential	0.6 V
T, temperature	343.15 K
p_a^0, anode side pressure	202650 Pa
p_c^0, cathode side pressure	202650 Pa

	Relative humidity		
	100%	75%	50%
$x_{H_2}^0$, anode feed hydrogen mole fraction	0.846	0.885	0.923
$x_{H_2O,a}^0$, anode feed water mole fraction	0.154	0.115	0.077
$x_{O_2}^0$, cathode feed oxygen mole fraction	0.178	0.186	0.194
$x_{H_2O,c}^0$, cathode feed water mole fraction	0.154	0.115	0.077
$x_{N_2}^0$, cathode feed nitrogen mole fraction	0.668	0.699	0.729

The fluxes of the components in and out of the GDE-channel control volume and the inlet mass flow rates create a boundary value problem in the third dimension (z). A simple variable step size Euler integration algorithm is used to solve this problem by integrating along the channel in z-direction.

$$N_i(k+1) = N_i(k) + h \times \frac{\mathrm{d}N_i(k)}{\mathrm{d}z} \tag{12}$$

where k is the grid point and $i = H_2$ and H_2O for the anode and O_2 and H_2O for the cathode and h is the step size in the z-direction.

The step size along the channel, h is determined such that the relative change of the molar flow rates of components are less than 2%. After step size refinements and accuracy checks, a 2% relative change criteria gave a reasonable balance between accuracy and computing time.

In addition to concentration and current profiles along the channel, overall power output is calculated by integrating the current density along the channel using the trapezoid rule and multiplying by the cell potential.

$$\text{Power} = V_{\text{cell}} \times \sum_{k=0}^{k-1} \frac{h \times (I^{\text{avg}}(k) + I^{\text{avg}}(k+1))}{2} \tag{13}$$

Overall power output is then used to calculate power density by dividing by the effective MEA area:

$$\text{power density} = \frac{\text{power}}{(W_{\text{sh}} + W_{\text{ch}}) \times L} \tag{14}$$

This integration algorithm is implemented in MATLAB® as an M-File which calls the FEMLAB® two-dimensional model. The integration along the channel required 30–70 two-dimensional model calls. The typical run times for each 2D simulation are 30–100 s, with the longer times for high current density operation. The total simulation times range between 30

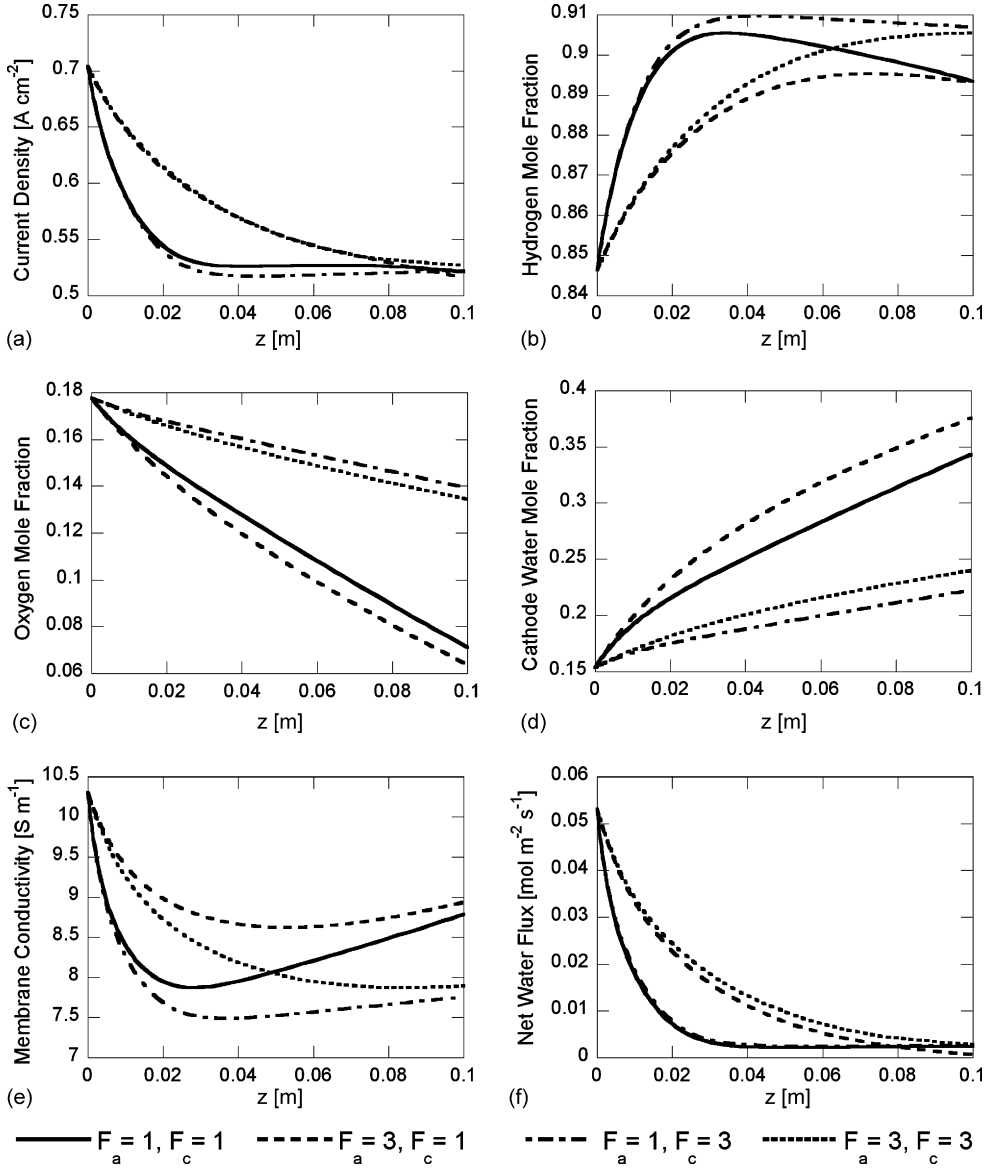

Fig. 3. Profiles along the channel for 100% relative humidity fuel and oxidant: (a) average current density, (b) average anode hydrogen mole fraction, (c) average cathode oxygen mole fraction, (d) average cathode water mole fraction, (e) average membrane conductivity, (f) average net water flux density.

and 70 min. The majority of the simulations for this problem were completed under 45 min on an Intel Pentium® 4 3.2 Ghz CPU with 1 GB of DDRam.

4. Results and discussions

The model was run for flow rates of 1 and 3 based at 1 A cm^{-2}, for both the anode (F_a) and the cathode sides (F_c), at three different humidification levels (100, 75, and 50% relative humidity) and at a fuel cell potential of 0.6 V. The geometric parameters of the fuel cell used are listed in Table 1. The fuel and oxidant flows are co-current in the flow channels. The operating conditions of the cell and the inlet composition of the fuel and oxidant are shown in Table 2. Fig. 3 shows the results for 100% RH hydrogen and air, Fig. 4 shows the results for 75% RH hydrogen and air, and Fig. 5 has the results for 50% RH case.

The average current density profile, calculated by Eq. (10), along a 10 cm long straight channel is shown in Fig. 3(a) for four different stoichiometric flow rates. This plot shows that increasing the hydrogen flow rate (F_a) from 1 to 3 increases the current density significantly, mostly because increasing the hydrogen flow rate also increases the amount of water supplied. More water in the anode feed hydrates the membrane causing higher membrane conductivity; Fig. 3(e) shows the increased membrane conductivity.

Fig. 3(b) is a plot of hydrogen mole fraction versus length. This confirms that the water concentration does increase with hydrogen flow ($F_a = 3$).

Increasing the air flow rate ($F_c = 3$) does not improve the current density but can actually decrease the performance slightly as shown in Fig. 3(a). Even though higher air flow maintains a higher oxygen concentration, the higher air flow prevents the concentration of water to increase on the cathode side. This

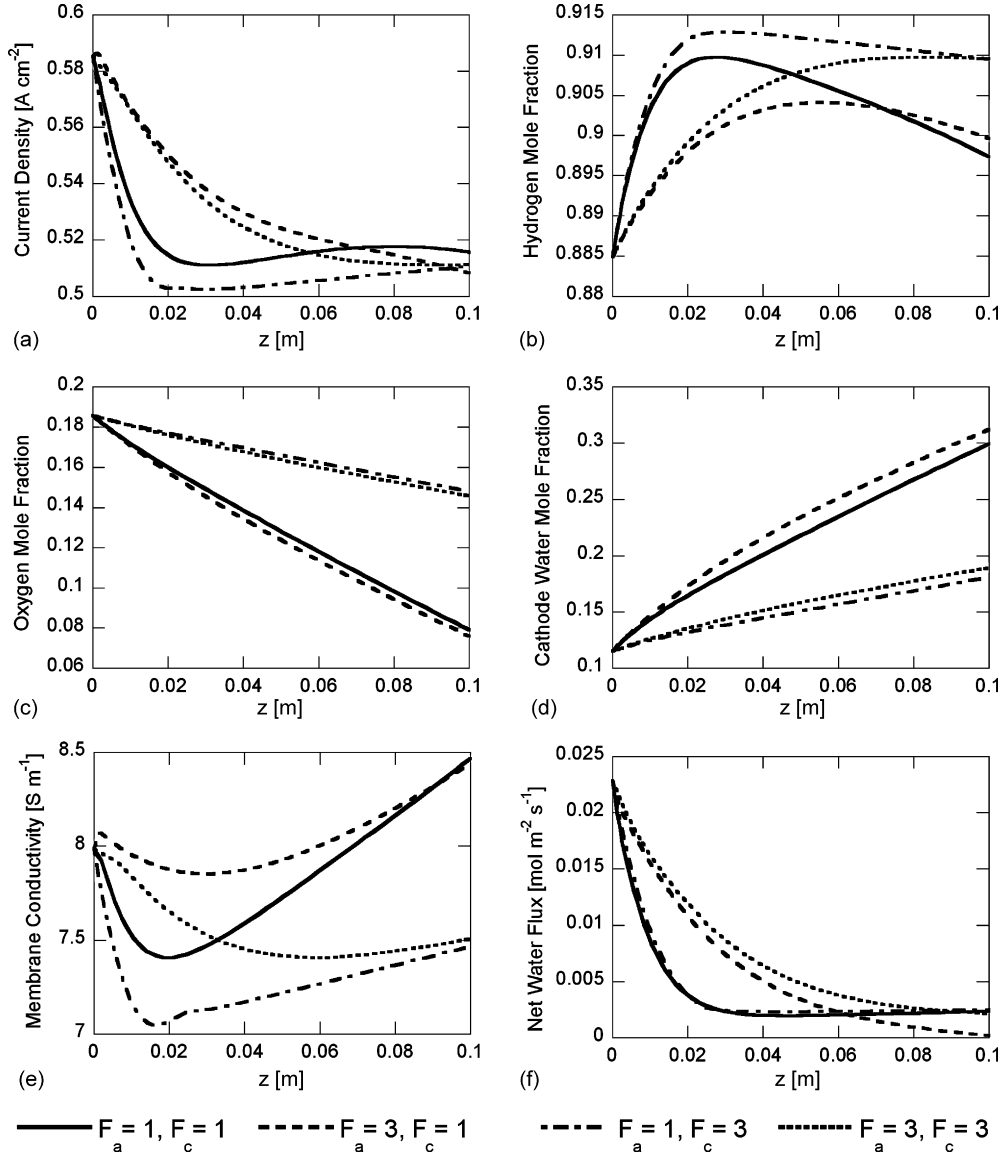

Fig. 4. Profiles along the channel for 75% relative humidity fuel and oxidant: (a) average current density, (b) average anode hydrogen mole fraction, (c) average cathode oxygen mole fraction, (d) average cathode water mole fraction, (e) average membrane conductivity, (f) average net water flux density.

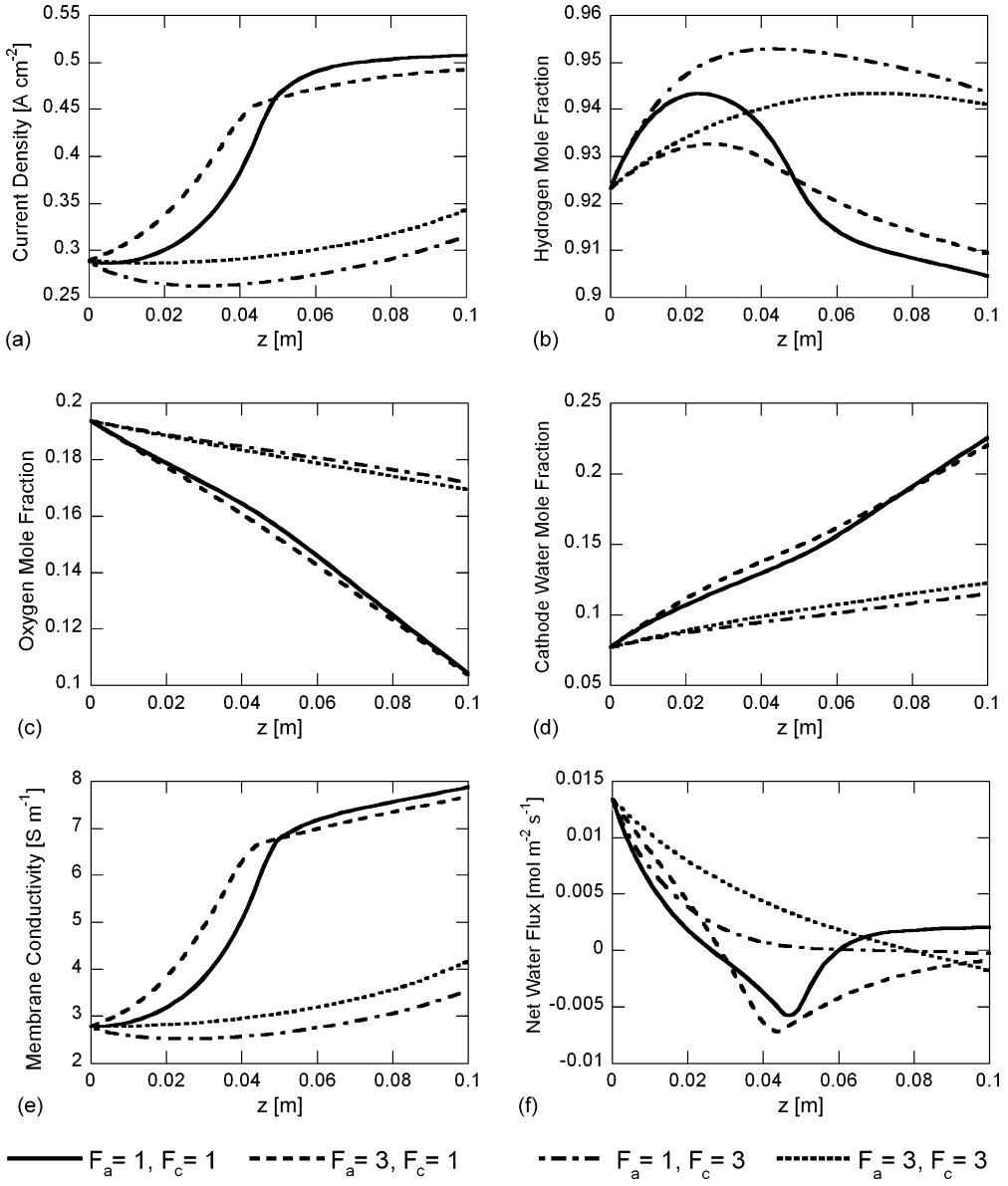

Fig. 5. Profiles along the channel for 50% relative humidity fuel and oxidant: (a) average current density, (b) average anode hydrogen mole fraction, (c) average cathode oxygen mole fraction, (d) average cathode water mole fraction, (e) average membrane conductivity, (f) average net water flux density.

is caused by the air removing water from the cathode channel (Fig. 3(d)). Lower water concentrations at the cathode side, causes less back diffusion of water from cathode to anode and thus lowers the membrane conductivity.

When the PEM fuel cell is operated at equal pressures at anode and cathode sides, water transport in the membrane is governed by only two processes: flow of water from anode to cathode due to electro-osmotic drag and the diffusion of water from higher to lower concentrations. The convective flux of water is zero inside the membrane due to the zero pressure gradient. Thus the water flux can be written as:

$$N_w = \frac{n_d \cdot \mathbf{I}}{F} - D_w \nabla c_w \quad (15)$$

where c_w is the concentration of water, D_w the diffusion coefficient of water in the membrane, n_d the electro-osmotic drag coefficient, $\mathbf{I}$ the local current density vector, and F is the Faraday constant.

Fig. 3(b) shows that the anode water mole fractions are between 0.09 and 0.15 (1 − anode hydrogen mole fraction), however on the cathode side the mole fraction of water ranges between 0.154 and 0.375 (Fig. 3 (d)). The net water flux in Fig. 3(f) is always positive meaning flow of water is from the anode to the cathode.

When the current density profiles for all four cases in Fig. 3(a) are compared it is interesting that the current densities converge to almost the same value at the exit. However hydrogen mole fraction values converge to a single value at the exit only for a given air flow rate (Fig. 3(b)). For example at $F_c = 1$ the hydrogen mole fractions converge to 0.893, and at $F_c = 3$ the hydrogen mole fractions converge to 0.906. This shows that water concentrations at the anode and the cathode sides reach equilibrium and

the equilibrium value appears to be a slight function of the air flow rates.

A lower equilibrium water concentration at the anode for the higher air flow rates $S_c = 3$ also confirms the water removal effect of air. Fig. 3(c) shows the mole fraction profile of oxygen along the cathode channel. The mole fraction of oxygen is almost linear along the channel. As expected, higher air flow rates result in a slower decrease of oxygen and higher exiting mole fractions. The oxygen mole fraction profiles show slight differences for the two hydrogen flow rates. The higher hydrogen flow rates ($F_a = 3$) causes more water to be transported to the cathode side thus lowering the mole fraction of oxygen.

The 75% RH hydrogen and air results are shown in Fig. 4. Similar to the 100% RH case, the cell performance can be improved by increasing the hydrogen flow rate as shown in Fig. 4(a). Also the water removal effect of the higher air flow rates on the cell performance is more noticeable for 75% RH (Fig. 4(d)) than for the 100% RH case due to lower water supply.

Fig. 4(a) shows that the current density at the entrance for the 75% RH cases is significantly lower than the 100% RH cases (Fig. 3(a)). This is caused by the higher membrane conductivity at the entrance 10.3 S m^{-1} for 100% RH versus 8 S m^{-1} for the 75% relative humidity (Figs. 3(e) and 4(e)).

Similar to the 100% RH case, the 75% RH case reaches an equilibrium water flux at the anode exit. As expected for all flow rates the conductivities are always lower for all lower RH cases. For $F_c = 3$ the back diffusion of water from cathode to anode is not high enough to keep the membrane hydrated at the entrance levels, due to the water removal effect of the higher air flow rate. For the $F_c = 1$ cases, membrane conductivities are higher at the exit than the entrance due to higher water concentrations obtained at the exit. This increase causes an increase in current density at approximately 2 cm from the entrance (Fig. 4(a)). Although the membrane conductivity starts increasing after the first 2 cm, it does not improve the current density significantly, because the concentration of oxygen also decreases rapidly at the exit.

Fig. 4(f) shows the net water flux through the membrane for 75% RH case. The net water flux at the entrance is less than half of the 100% RH case mainly because higher current densities at 100% RH, moves more water from anode to cathode due to electro-osmotic drag.

Although the 100 and 75% RH case performances show similarities, the results for 50% RH are significantly different (Fig. 5). The entrance current density is 0.3 A cm^{-2} for the 50% RH case which is significantly lower than the 100 and 75% RH cases of 0.70 and 0.58 A cm^{-2}, respectively. This is due to the very low conductivity of the membrane at the entrance (2.9 S m^{-1}). As the water produced at the cathode side increases, the membrane becomes more hydrated and its conductivity increases. This increases the current density along the channel as shown in Fig. 5(a). Similar to the 100 and 75% RH cases, increasing hydrogen flow rates improved the performance for the 50% RH cases for the first half of the channel; however after 5 cm, the performance of $F_a = 1$ ($F_c = 1$) is better than $F_a = 3$ ($F_c = 1$). For the 50% RH case, high air flow rates significantly decrease the current density and membrane conductivity due to the water removal effect of the high flow rates. In general the low overall performance of 50% RH case is caused by the membrane not being properly hydrated, making it an undesired operating condition.

For both the 100 and 75% RH cases the net water fluxes are from anode to cathode; however Fig. 5(f) shows the water flux changes from anode to cathode (positive) to cathode to anode (negative) after the first 3 cm of the channel. This is caused by the concentration of water increasing at the anode due to increased consumption of hydrogen causing back diffusion of water from the cathode.

4.1. Flooding concerns

At 343.15 K and 2 atm, water will condense when the mole fraction of water exceeds 0.154. Fig. 3(d) shows that water could condense throughout the cathode for 100% RH and it will start condensing after the first 1.3 cm of the fuel cell cathode channel for the 75% RH case. Pasaogullari and Wang [18] showed that electrode flooding will occur when current densities are higher than 1.4 A cm^{-2} at 100% RH hydrogen and air. This is significantly higher than the current densities studied in this work. Also in the Pasaogullari and Wang [18] work water activity levels (p_w/p_w^{sat}) exceeded 3 in severe flooding cases, whereas the highest water activity level in this work is 2.4. It is uncertain that whether electrode flooding will occur in the cases shown in Figs. 3 and 4, however our higher GDE porosity of 0.6 versus 0.5 of Pasaogullari and Wang [18], as well as our lower current densities, suggest that flooding may not occur.

Figs. 6 and 7 show the power density calculated by Eq. (14), versus hydrogen utilization (varying F_a) for 100 and 75% RH. For both 100 and 75% RH cases the power density decreases with increasing hydrogen utilization (decreasing F_a). The relative magnitude of this decrease is higher for 100% RH than for 75% RH. Higher hydrogen flow rates (increasing F_a) show improved performance by providing more water and maintaining higher membrane hydration levels along the channel. However higher F_a's decrease hydrogen utilization, requiring hydrogen

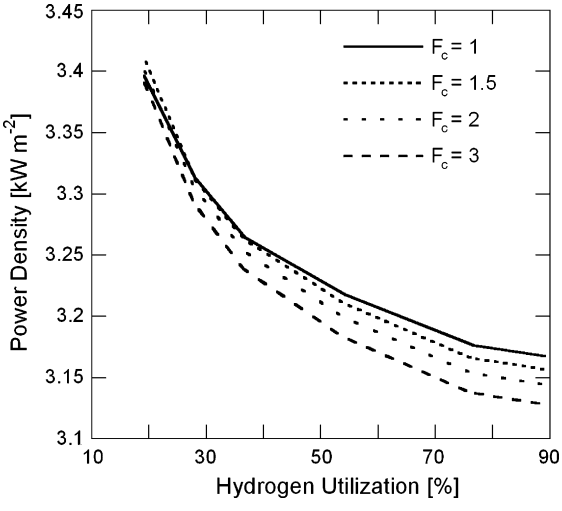

Fig. 6. Power density and hydrogen utilization for 100% RH fuel and oxidant.

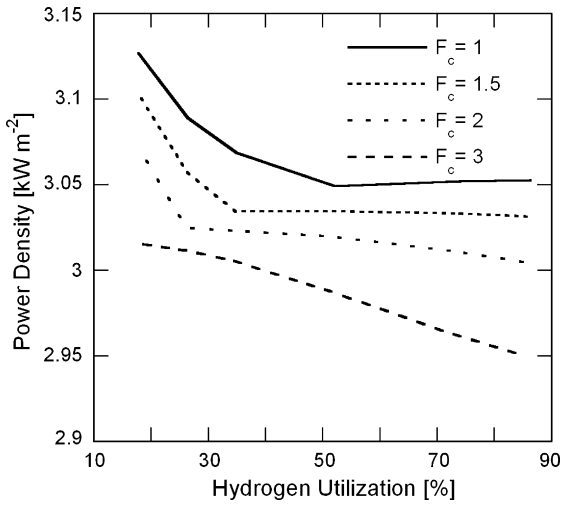

Fig. 7. Power density and hydrogen utilization for 75% RH fuel and oxidant.

recycling to maintain the fuel cell system efficiency. For both 100 and 75% RH, increasing air flow rate decreases the power density more for high hydrogen utilizations. The effect of increasing air flow rates is less at low hydrogen utilizations because the power density is higher thus more water is generated at the cathode compared to high hydrogen utilization. With more water generated at low hydrogen utilization the water removal effect of increasing air flow rates is smaller.

5. Conclusions

A new algorithm is presented to obtain three-dimensional results from a two-dimensional PEMFC model. A simple Euler integration method is used to solve the component balances along the fuel cell channels that uses a two-dimensional, across-the-channel, finite element model for local current density and water flux values.

It was found that high hydrogen flow rates and low air flow rates performed better for both 100 and 75% RH cases. This is due to the water concentration in the membrane and the resulting high membrane conductivity. For these RH cases the net water flux was from anode to cathode as the electro-osmotic drag exceeded the diffusive flux. Increasing the flow of hydrogen improved the performance due to more water supplied to the anode side where it is needed most for humidification of the membrane. Higher hydrogen flow rates also resulted in lower utilization of hydrogen thus requiring hydrogen recycle for overall system efficiency. Increasing air flow rates lowered the performance for the studied conditions, as high air flow rates remove the generated water quickly and does not allow the concentration of water to build up at the cathode to hydrate the membrane.

The low performance for hydrogen and air at 50% RH showed that the membrane is not properly hydrated. Even though the water concentration near the exit and the membrane conductivity increases, the performance of hydrogen and air with 50% RH is poor compared to 100 and 75% RH.

The 100% RH case had a power density of 3.23 kW m^{-2} at $F_c = 1$ with 50% hydrogen utilization; however, the maximum power density of 75% RH operation at $F_c = 1$ with 50% hydrogen utilization is 3.05 kW m^{-2}. This is a 5.6% decrease in the power density due to lower humidification. As the hydrogen utilization increases, the difference between 100 and 75% RH operation power densities decreases. Operation at 75% RH gave a more uniform current density profile compared to 100% RH. Uniform current density in the PEMFC's is desired to enhance thermal management, reliability and fuel cell life. Non-uniformities in current density can create hot spots due to local heat generation which can damage the membrane permanently. The 75% RH results show the trade off between performance and reliability which must be optimized to meet application requirements.

The model used in these calculations assumes a single vapor phase thus liquid water formation and electrode flooding cannot be addressed. However when compared to the two-phase models reported in the literature that show electrode flooding, the water activity levels reached in this study are below reported flooding values.

This study shows that the relative humidity of the hydrogen and the air, as well as their flow rates, are critical for the reliability, i.e. uniform current density, and power output. Air flow rate and relative humidity of air must be controlled to prevent membrane dry-out and electrode flooding. To study the extreme cases of electrode flooding a two-phase model should be used in the electrodes.

The integration algorithm used in this work is the first attempt to combine a state-of-the-art finite element model with Euler integration to simulate a three-dimensional fuel cell. This new approach when compared to other three-dimensional CFD models is much faster. With a detailed two-dimensional across-the-channel model, as used in this study, the effects of channel and shoulder dimensions can be studied. The order of magnitude differences in the characteristic dimensions of a PEMFC makes this approach more suitable. It has been shown in our previous work [14] that the concentration of reactants can change more than 90% under the bipolar plate shoulders for 1 mm channel and shoulder sizes. However due to the high flow rates in channels only a 2% concentration change can be seen in 0.2–3 mm of channel length depending on operating conditions. Thus the rate of change of composition along the channel is small compared to that observed across the channel, validating our approach.

This approach can be used for estimating overall PEMFC performance for co-current flow and parallel channel design. Also with an iterative procedure it could be used for counter-current flow as well as different channel layouts.

References

[1] EG&G Technical Services, Inc., Fuel Cell Handbook, sixth ed., DOE NETL, 2002.
[2] S. Gottesfeld, T. Zawodzinski, Adv. Electrochem. Sci. Eng. 5 (1997) 195–301.
[3] V. Mehta, J.S. Cooper, J. Power Sources 114 (2003) 32–53.
[4] K. Haraldsson, K. Wipke, J. Power Sources 126 (2004) 88–97.
[5] D.M. Bernardi, M.W. Vebrunge, J. Electrochem. Soc. 139 (9) (1992) 2477–2491.
[6] T.E. Springer, T.A. Zawodzinski, S. Gottesfeld, J. Electrochem. Soc. 138 (8) (1991) 2334–2342.

[7] T.F. Fuller, J. Newman, J. Electrochem. Soc. 140 (5) (1993) 1218–1225.
[8] V. Gurau, H. Liu, S. Kakac, AIChE J. 44 (11) (1998) 2410–2422.
[9] S. Um, C.Y. Wang, J. Power Sources 125 (2004) 40–51.
[10] S. Dutta, S. Shimpalee, J.W. Van Zee, App. Electrochem 30 (2000) 135–146.
[11] T. Berning, D.M. Lu, N. Djilali, J. Power Sources 106 (2002) 284–294.
[12] P.T. Nguyen, T. Berning, N. Djilali, J. Power Sources 130 (2004) 149–157.
[13] H. Meng, C.Y. Wang, Chem. Eng. Sci. 59 (2004) 3331–3343.
[14] G.H. Guvelioglu, H.G. Stenger, J. Power Sources 147 (2005) 95–106.
[15] G.H. Guvelioglu, H.G. Stenger, J. Power Sources 156 (2006) 424–433.
[16] T. Berning, N. Djilali, J. Power Sources 124 (2003) 440–452.
[17] T. Berning, N. Djilali, J. Electochem. Soc. 150 (12) (2003) A1598–A1607.
[18] U. Pasaogullari, C.Y. Wang, J. Electrochem. Soc. 152 (2005) A380–A390.
[19] J. Larminie, A. Dicks, Fuel Cell Systems Explained, Wiley, Chichester, 2000.
[20] MATLAB 7. 0, The MathWorks Inc., Natick, MA, 2004.
[21] R.H. Perry, D.W. Green, Perry's Chemical Engineer's Handbook, seventh ed., McGraw-Hill, 1997.